# Supplemental Data

## Haplotype Reference Consortium Affiliations and Additional WHI Acknowledgment

**Haplotype Reference Consortium:** http://www.haplotype-reference-consortium.org/

**Human Genetics, Wellcome Trust Sanger Institute, Hinxton, UK.**
Shane McCarthy, Yang Luo, Arthur Gilly, Jeffrey C Barrett, Eleftheria Zeggini, Nicole Soranzo, Klaudia Walter, Carl A Anderson & Richard Durbin

**Department of Biostatistics, University of Michigan, Ann Arbor, Michigan, USA.**
Sayantan Das, Hyun Min Kang, Christian Fuchsberger, Alan Kwong, Laura J Scott, Sai Chen, Michael Boehnke & Gonçalo Abecasis

**Center for Statistical Genetics, University of Michigan, Ann Arbor, Michigan, USA.**
Sayantan Das, Hyun Min Kang, Christian Fuchsberger, Alan Kwong, Laura J Scott, Sai Chen, Michael Boehnke, Gonçalo Abecasis

**Wellcome Trust Centre for Human Genetics, University of Oxford, Oxford, UK.**
Warren Kretzschmar, Anubha Mahajan, Mark I McCarthy, Jonathan Marchini

**Genetics and Development, University of Geneva, Geneva, Switzerland.**
Olivier Delaneau

**Genetics of Complex Traits, Institute of Biomedical Science, University of Exeter Medical School, Exeter, UK.**
Andrew R Wood, Marcus Tuke & Timothy Frayling

**Institute for Community Medicine, University Medicine Greifswald, Greifswald, Germany.**
Alexander Teumer

**DZHK (German Centre for Cardiovascular Research), Greifswald, Germany.**
Alexander Teumer, Matthias Nauck

**Vertebrate Resequencing Informatics, Wellcome Trust Sanger Institute, Hinxton, UK.**
Petr Danecek

**Department of Statistics, University of Oxford, Oxford, UK.**
Kevin Sharp, Jonathan Marchini

**IRGB, CNR, Sardinia, Italy.**
Carlo Sidore, Andrea Angius, Fabio Busonero, Francesco Cucca

**MRC Integrative Epidemiology Unit, University of Bristol, Oakfield Grove, UK.**
Nicholas Timpson, Laura J Corbin, George Davey Smith, Josine L Min

**THL, Helsinki, Finland.**
Seppo Koskinen, Veikko Salomaa

**Institute for Behavioral Genetics, University of Colorado, Boulder, Colorado, USA.**
Scott Vrieze

**Department of Psychology and Neurosurgery, University of Colorado, Boulder, Colorado, USA.**
Scott Vrieze

**Division of Cardiovascular Medicine, Department of Internal Medicine, University of Michigan, Ann Arbor, Michigan, USA.**
He Zhang, Cristen Willer

**Department of Neurology and Neurosurgery, Brain Center Rudolf Magnus, Utrecht, the Netherlands.**
Jan Veldink, Leonard H Van den Berg, Wouter Van Rheenen, Annelot Dekker

**Public Health Sciences Division, Fred Hutchinson Cancer Research Center, Seattle, Washington, USA.**
Ulrike Peters, Tabitha Harrison, Charles Kooperberg

**Department of Epidemiology, University of Washington School of Public Health, Seattle, Washington, USA.**
Ulrike Peters

**Department of Psychiatry, SUNY Downstate, Brooklyn, New York, USA.**
Carlos Pato, Michele Pato

**Genetic Epidemiology Unit, Department of Epidemiology, Erasmus MC, Rotterdam, the Netherlands.**
Cornelia M van Duijn

**Department of Pediatrics–Nephrology, University of Michigan School of Medicine, Ann Arbor, Michigan, USA.**
Christopher E Gillies, Matthew G Sampson

**Department of Medical, Surgical and Health Sciences, University of Trieste, Trieste, Italy.**
Ilaria Gandin, Massimiliano Cocca, Nicola Pirastu, Paolo Gasparini

**Genetica Medica, IRCCS Burlo Garofolo, Trieste, Italy.**
Massimo Mezzavilla

**Department of Experimental Genetics, Sidra, Doha, Qatar.**
Massimo Mezzavilla, Paolo Gasparini

**Genetics and Cell Biology, San Raffaele Research Institute, Milan, Italy.**
Michela Traglia, Cinzia Sala, Daniela Toniolo

**Netherlands Twin Register, Department of Biological Psychology, Vrije Universiteit Amsterdam, Amsterdam, the Netherlands.**
Dorrett Boomsma

**Department of Ophthalmology and Visual Sciences, University of Michigan, Ann Arbor, Michigan, USA.**
Kari Branham

**MRC Social Genetic and Developmental Psychiatry Centre, Institute of Psychiatry, Psychology and Neuroscience, King's College London, London, UK.**
Gerome Breen

**NIHR Biomedical Research Centre for Mental Health, Institute of Psychiatry, Psychology and Neuroscience, King's College London and the South London Maudsley Hospital, London, UK.**
Gerome Breen

**Department of Anesthesiology, University of Michigan, Ann Arbor, Michigan, USA.**
Chad M Brummett, Ross M Fraser

**Usher Institute of Population Health Sciences and Informatics, University of Edinburgh, Edinburgh, UK.**
Harry Campbell, James F Wilson

**Usher Institute of Population Health Sciences and Informatics, University of Edinburgh, Edinburgh, UK.**
Andrew Chan

**Channing Division of Network Medicine, Brigham and Women's Hospital, Boston, Massachusetts, USA.**
Andrew Chan

**Department of Computational Medicine, University of Michigan, Ann Arbor, Michigan, USA.**
Sai Chen, Matthias Kretzler, Cristen Willer

**Department of Bioinformatics, University of Michigan, Ann Arbor, Michigan, USA.**
Sai Chen, Matthias Kretzler, Cristen Willer

**Division of Epidemiology and Clinical Applications, National Eye Institute, Bethesda, Maryland, USA.**
Emily Chew

**Medical Genomics and Metabolic Genetics Branch, National Human Genome Research Institute, US National Institutes of Health, Bethesda, Maryland, USA.**
Francis S Collins

**Department of Nutrition and Dietetics, School of Health Science and Education, Harokopio University, Athens, Greece.**
George Dedoussis, Aliki-Eleni Farmaki

**Department of Internal Medicine B, University Medicine Greifswald, Greifswald, Germany.**
Marcus Dorr

**Institute of Clinical Chemistry and Laboratory Medicine, University Medicine Greifswald, Greifswald, Germany.**
Marcus Dorr, Matthias Nauck, Uwe Volker

**Longitudinal Studies Section, Clinical Research Branch, Gerontology Research Center, National Institute on Aging, Baltimore, Maryland, USA.**
Luigi Ferrucci

**Division of Genetic Epidemiology, Department of Medical Genetics, Molecular and Clinical Pharmacology, Medical University of Innsbruck, Innsbruck, Austria.**
Lukas Forer, Sebastian Schoenherr

**Program in Medical and Population Genetics, Broad Institute of MIT and Harvard, Cambridge, Massachusetts, USA.**
Stacey Gabriel, Aarno Palotie, David Altshuler

**HudsonAlpha Institute for Biotechnology, Huntsville, Alabama, USA.**
Shawn Levy, Richard M Myers

**Department of Clinical Sciences, Diabetes and Endocrinology, University of Lund, Malmö, Sweden.**
Leif Groop

**Finnish Institute for Molecular Medicine, University of Helsinki, Helsinki, Finland.**
Leif Groop

**Research Programs Unit, Diabetes and Obesity, University of Helsinki, Helsinki, Finland.**
Leif Groop

**Institute of Biomedical and Clinical Research, University of Exeter Medical School, Exeter, UK.**
Andrew Hattersley

**Hunt Research Centre, Department of Public Health and General Practice, Norwegian University of Science and Technology, Levanger, Norway.**
Oddgeir L Holmen, Kristian Hveem

**Department of Internal Medicine, University of Michigan School of Medicine, Ann Arbor, Michigan, USA.**
Matthias Kretzler

**Cambridge Institute for Medical Research, University of Cambridge, Cambridge, UK.**
James C Lee

**Department of Medicine, University of Cambridge School of Clinical Medicine, Addenbrooke's Hospital, Cambridge, UK.**
James C Lee

**Department of Psychology, University of Minnesota, Minneapolis, Minnesota, USA.**
Matt McGue, William Iacono

**Institute of Human Genetics, Helmholtz Zentrum München–German Research Center for Environmental Health, Neuherberg, Germany.**
Thomas Meitinger

**Institute of Human Genetics, Technische Universität München, Munich, Germany.**
Thomas Meitinger

**DZHK (German Centre for Cardiovascular Research), Partner Site Munich Heart Alliance, Munich, Germany.**
Thomas Meitinger

**Epidemiology and Public Health, Institute of Biomedical and Clinical Science, University of Exeter Medical School, Exeter, UK.**
David Melzer

**Department of Genetics, University of North Carolina at Chapel Hill, Chapel Hill, North Carolina, USA.**
Karen L Mohlke

**Molecular Neuropsychiatry and Development Laboratory, Centre for Addiction and Mental Health, Toronto, Ontario, Canada.**
John B Vincent

**Department of Psychiatry, University of Toronto, Toronto, Ontario, Canada.**
John B Vincent

**Institute of Medical Science, University of Toronto, Toronto, Ontario, Canada.**
John B Vincent

**Department of Genome Sciences, University of Washington, Seattle, Washington, USA.**
Deborah Nickerson

**Institute for Molecular Medicine, FIMM, Helsinki, Finland.**
Aarno Palotie

**Analytic and Translational Genetics Unit, Department of Medicine, Massachusetts General Hospital, Boston, Massachusetts, USA.**
Aarno Palotie

**Stanley Center for Psychiatric Research, Broad Institute of MIT and Harvard, Cambridge, Massachusetts, USA.**
Aarno Palotie, David Altshuler

**Psychiatric and Neurodevelopmental Genetics Unit, Department of Psychiatry, Massachusetts General Hospital, Boston, Massachusetts, USA.**
Aarno Palotie

**Department of Neurology, Massachusetts General Hospital, Boston, Massachusetts, USA.**
Aarno Palotie

**Department of Psychiatry, University of Michigan, Ann Arbor, Michigan, USA.**
Melvin McInnis

**Department of Medicine, McGill University, Montreal, Quebec, Canada.**
J Brent Richards

**Department of Human Genetics, McGill University, Montreal, Quebec, Canada.**
J Brent Richards

**Department of Twin Research and Genetic Epidemiology, King's College London, London, UK.**
J Brent Richards, Kerrin Small, Timothy Spector

**National Institute on Aging, US National Institutes of Health, Baltimore, Maryland, USA.**
David Schlessinger

**Molecular Epidemiology Section, Department of Medical Statistics and Bioinformatics, Leiden University Medical Center, Leiden, the Netherlands.**
P Eline Slagboom

**Department of Ophthalmology, University of Pennsylvania, Philadelphia, Pennsylvania, USA.**
Dwight Stambolian

**Chronic Disease Prevention Unit, National Institute for Health and Welfare, Helsinki, Finland.**
Jaakko Tuomilehto

**Dasman Diabetes Institute, Dasman, Kuwait.**
Jaakko Tuomilehto

**Center for Vascular Prevention, Danube University Krems, Krems, Austria.**
Jaakko Tuomilehto

**Diabetes Research Group, King Abdulaziz University, Jeddah, Saudi Arabia.**
Jaakko Tuomilehto

**Interfaculty Institute for Genetics and Functional Genomics, University Medicine Greifswald, Greifswald, Germany.**
Uwe Volker

**Department of Genetics, University of Groningen, University Medical Center Groningen, Groningen, the Netherlands.**
Cisca Wijmenga, Morris A Swertz

**MRC Human Genetics Unit, Institute of Genetics and Molecular Medicine, University of Edinburgh, Western General Hospital, Edinburgh, UK.**
James F Wilson

**Medical Genetics, University Medical Center Utrecht, Utrecht, the Netherlands.**
Paul I W de Bakker

**Department of Genetics, Center for Molecular Medicine, University Medical Center Utrecht, Utrecht, the Netherlands.**
Paul I W de Bakker

**University of Groningen, University Medical Center Groningen, Genomics Coordination Center, Groningen, the Netherlands.**
Morris A Swertz

**Department of Genetics, Harvard Medical School, Boston, Massachusetts, USA.**
Steven McCarroll

**Department of Molecular Biology, Massachusetts General Hospital, Boston, Massachusetts, USA.**
Steven McCarroll

**Diabetes Research Center (Diabetes Unit), Department of Medicine, Massachusetts General Hospital, Boston, Massachusetts, USA.**
David Altshuler

**Department of Medicine, Harvard Medical School, Boston, Massachusetts, USA.**
David Altshuler

**Department of Biology, Massachusetts Institute of Technology, Cambridge, Massachusetts, USA.**
David Altshuler

**Vertex Pharmaceuticals, Boston, Massachusetts, USA.**
David Altshuler

**Department of Public Health, University of Helsinki, Helsinki, Finland.**
Samuli Ripatti

**Department of Haematology, University of Cambridge, Cambridge, UK.**
Nicole Soranzo

**NIHR Blood and Transplant Unit (BTRU) in Donor Health and Genomics, University of Cambridge, Cambridge, UK.**
Nicole Soranzo

**Neurobiology–Neurodegeneration and Repair Laboratory, National Eye Institute, US National Institutes of Health, Bethesda, Maryland, USA.**
Anand Swaroop

**Oxford Centre for Diabetes, Endocrinology and Metabolism, Radcliffe Department of Medicine, University of Oxford, Oxford, UK.**
Mark I McCarthy

**Oxford NIHR Biomedical Research Centre, Churchill Hospital, Headington, Oxford, UK.**
Mark I McCarthy

**WHI Acknowledgment:**
*The WHI program is funded by the National Heart, Lung, and Blood Institute, National Institutes of Health, U.S. Department of Health and Human Services through contracts HHSN268201600018C, HHSN268201600001C, HHSN268201600002C, HHSN268201600003C, and HHSN268201600004C. The authors thank the WHI investigators and staff for their dedication, and the study participants for making the program possible. A full listing of WHI investigators can be found at: http://www.whi.org/researchers/Documents%20%20Write%20a%20Paper/WHI%20Investigator%20Long%20List.pdf*

**Supplemental Figures**

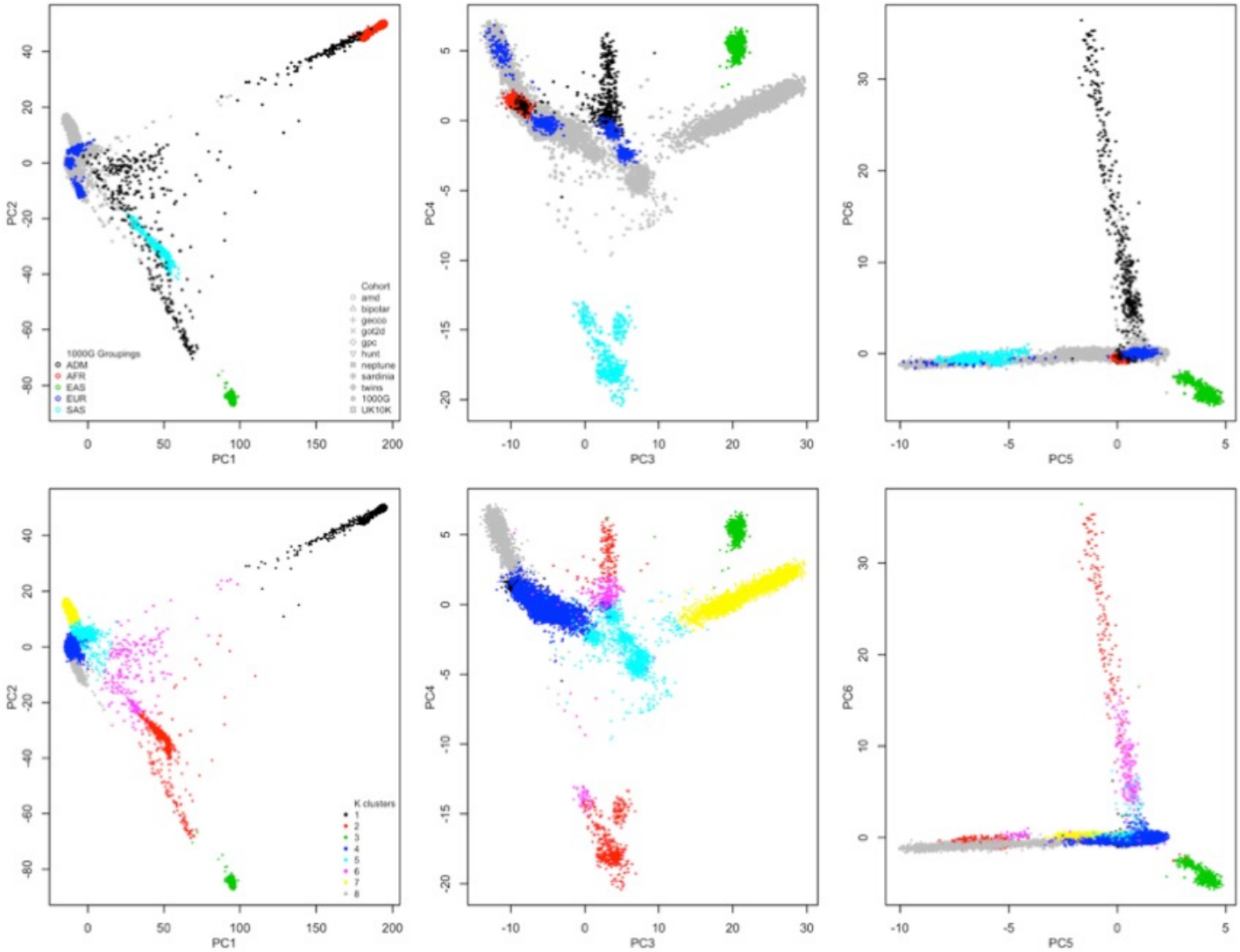


Figure S1. Principal components analysis of the HRC data using unlinked, common SNPs, showing 1000 Genomes populations and HRC sequencing cohorts (A-C) and the k-means clustering used to identify individuals of primarily European individuals. The European individuals were chosen from K=8 clusters, with EUR individuals identified as clusters 4, 5, 7, & 8 to exclude the majority of AFR, EAS, ADM, and SAS, while retaining a core set of EUR. We stress that this was not meant to be a perfect ancestry assignment procedure, only to identify a group of individuals of roughly EUR ancestry, from which subsamples of varying stratification could be identified.

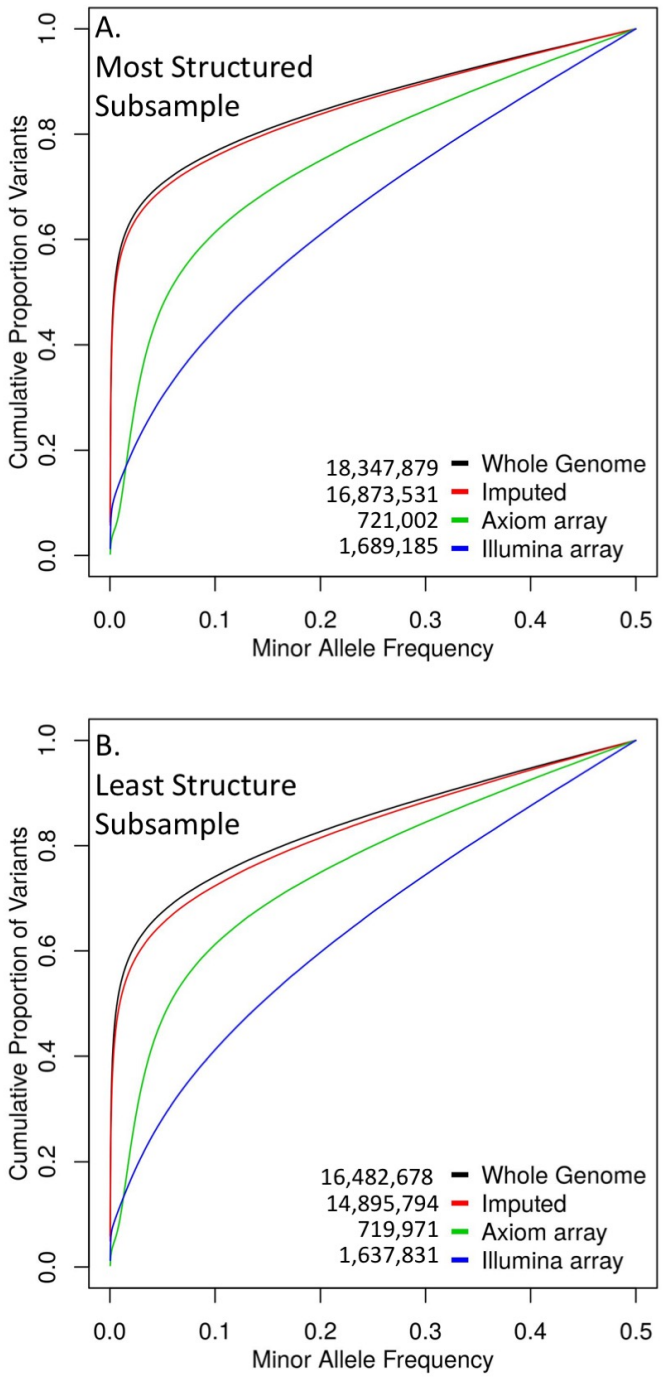


Figure S2. Cumulative distribution of minor allele frequency in the most structured subsample (A) and the lest structured subsample (B) for each of the different data types. Shown are the total number of variants in each dataset.

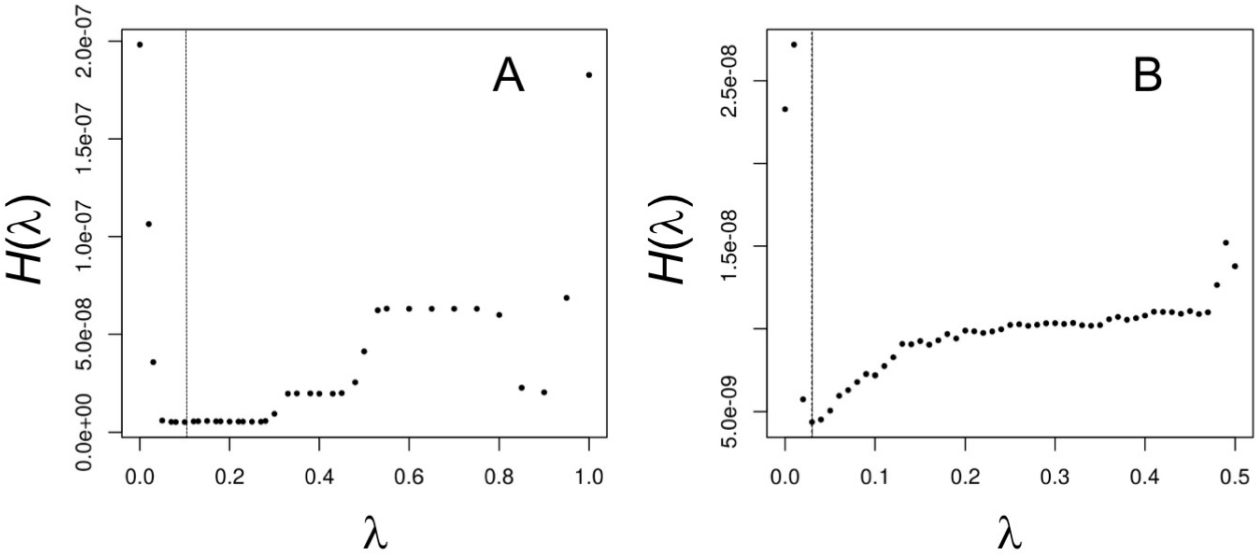


Figure S3. The marker subsampling method proposed by Crossett et al. (2013) to tune the smoothing parameter, λ. The weighted risk function, $H(\lambda)$, is shown as a function of λ, with the vertical dashed line representing the optimal value. Shown are two representative examples of the subsample and dataset combinations used in the analyses. (A) depicts data from the low structure subsample using array position SNPs, while (B) represents the most structured subsample using whole genome sequence data.

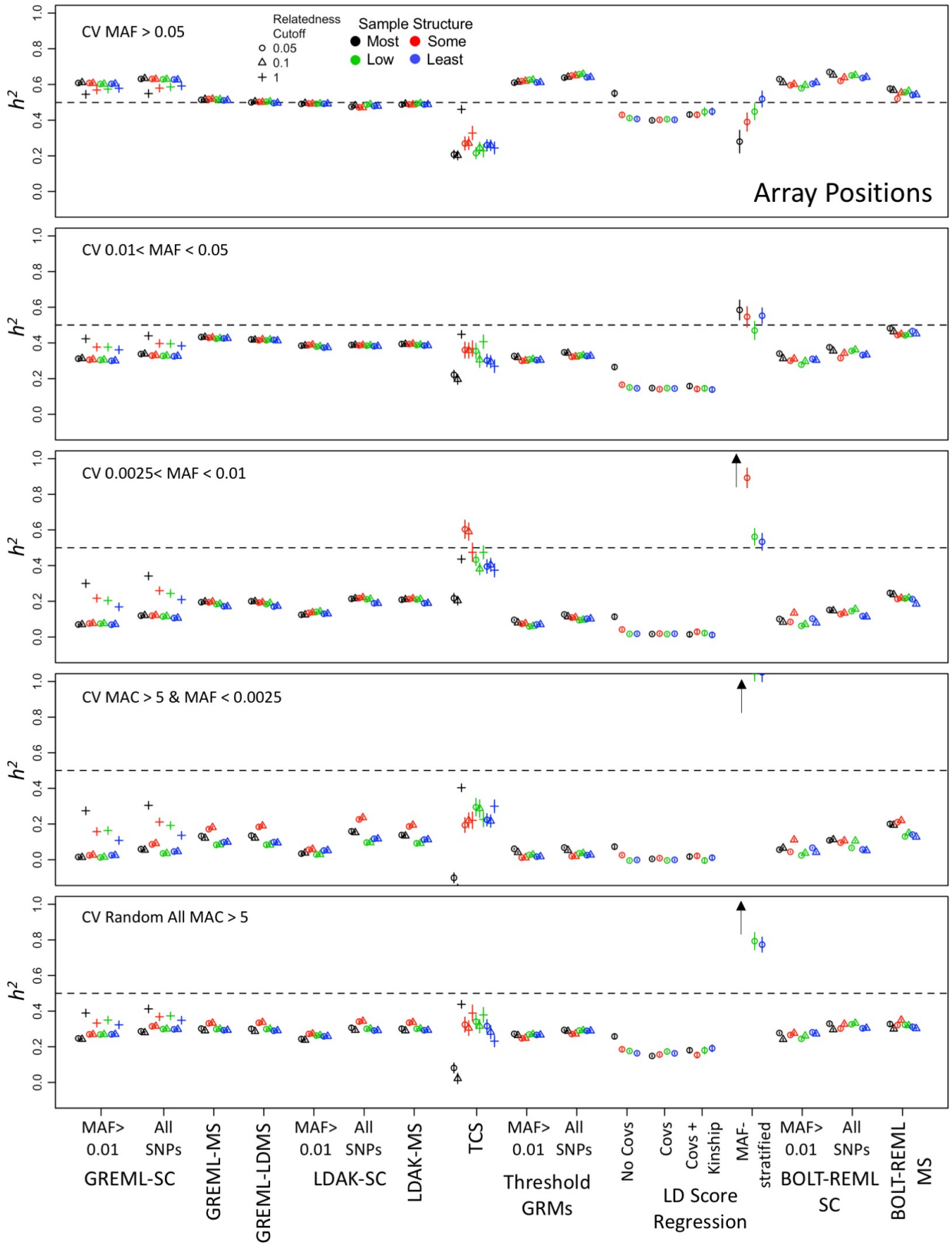


Figure S4. Narrow-sense heritability ($h^2$) estimates using Axiom array positions. Each horizontal panel indicates the minor allele frequency (MAF) range of the 1,000 randomly chosen causal variants (CV), with the range specified in the inset. Methods are listed on the X-axis as follows: Single component GREML (GREML-SC), MAF-stratified GREML (GREML-MS), LD- & MAF-stratified GREML (GREML-LDMS), Single-component Linkage Disequilibrium-Adjusted Kinships (LDAK-SC), MAF-stratified LDAK (LDAK-MS), Treelet Covariance Smoothing (TCS), Extended Genealogy with Thresholded GRMs, and LD Score Regression using no PCs as covariates in GWAS or using PCs as covariates, and BOLT-REML. Symbols represent different relatedness cutoffs (or threshold, *t*, using the Threshold GRMs method). Dotted line is the simulated (true) $h^2 = 0.5$. Mean (±SEM) of 100 replicates shown. Colors represent the 4 subsamples varying in genetic structure. Estimates >1 are indicated by arrow.

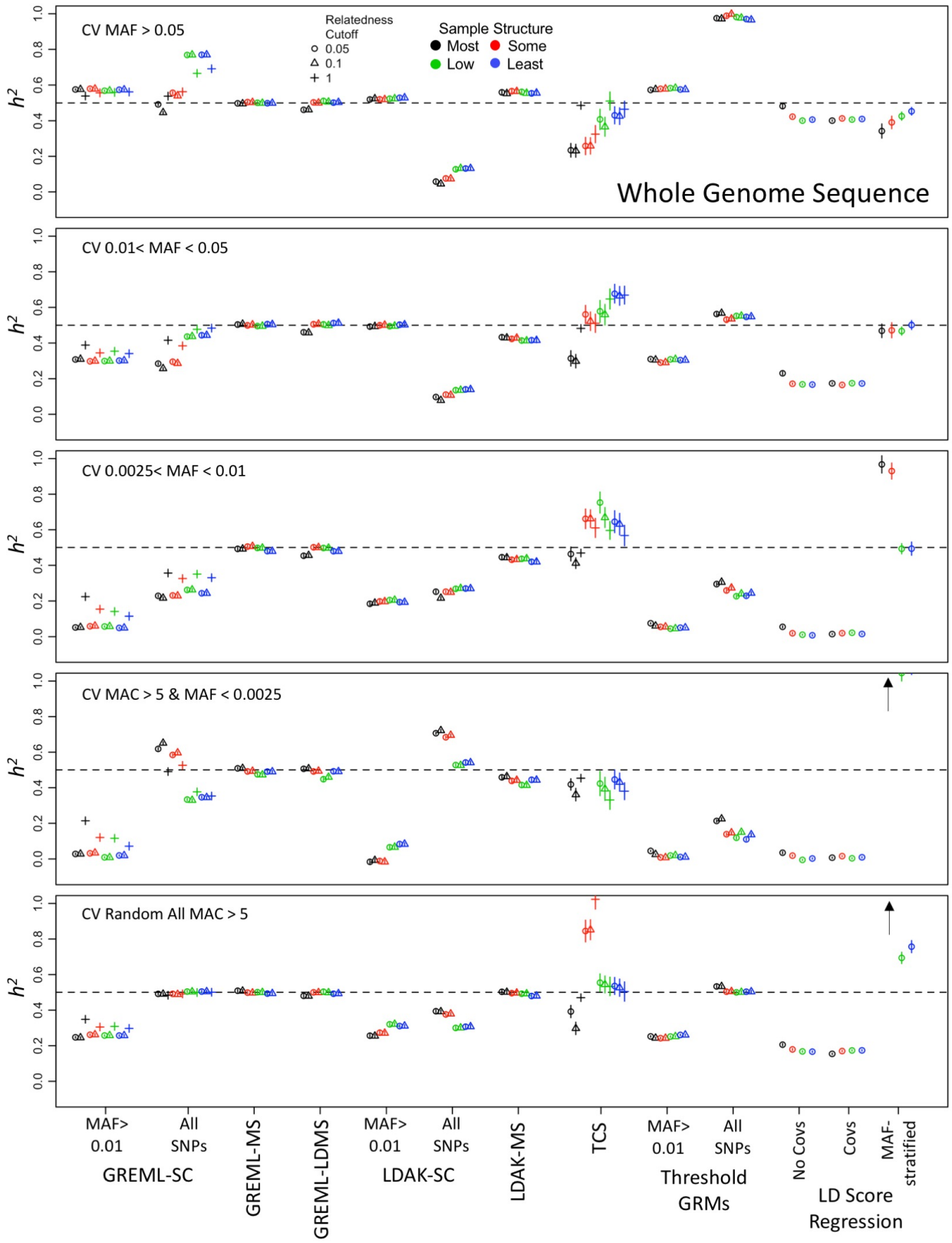


Figure S5. Narrow-sense heritability ($h^2$) estimates using whole genome sequence data. Each horizontal panel indicates the minor allele frequency (MAF) range of the 1,000 randomly chosen causal variants (CV), with the range specified in the inset. Methods are listed on the X-axis as follows: Single component GREML (GREML-SC), MAF-stratified GREML (GREML-MS), LD- & MAF-stratified GREML (GREML-LDMS), Single-component Linkage Disequilibrium-Adjusted Kinships (LDAK-SC), MAF-stratified LDAK (LDAK-MS), Treelet Covariance Smoothing (TCS), Extended Genealogy with Thresholded GRMs, and LD Score Regression using no PCs as covariates in GWAS or using PCs as covariates. Symbols represent different relatedness cutoffs (or threshold, *t*, using the Threshold GRMs method). Dotted line is the simulated (true) $h^2 = 0.5$. Mean (±SEM) of 100 replicates shown. Colors represent the 4 subsamples varying in genetic structure. Estimates >1 are indicated by arrow.

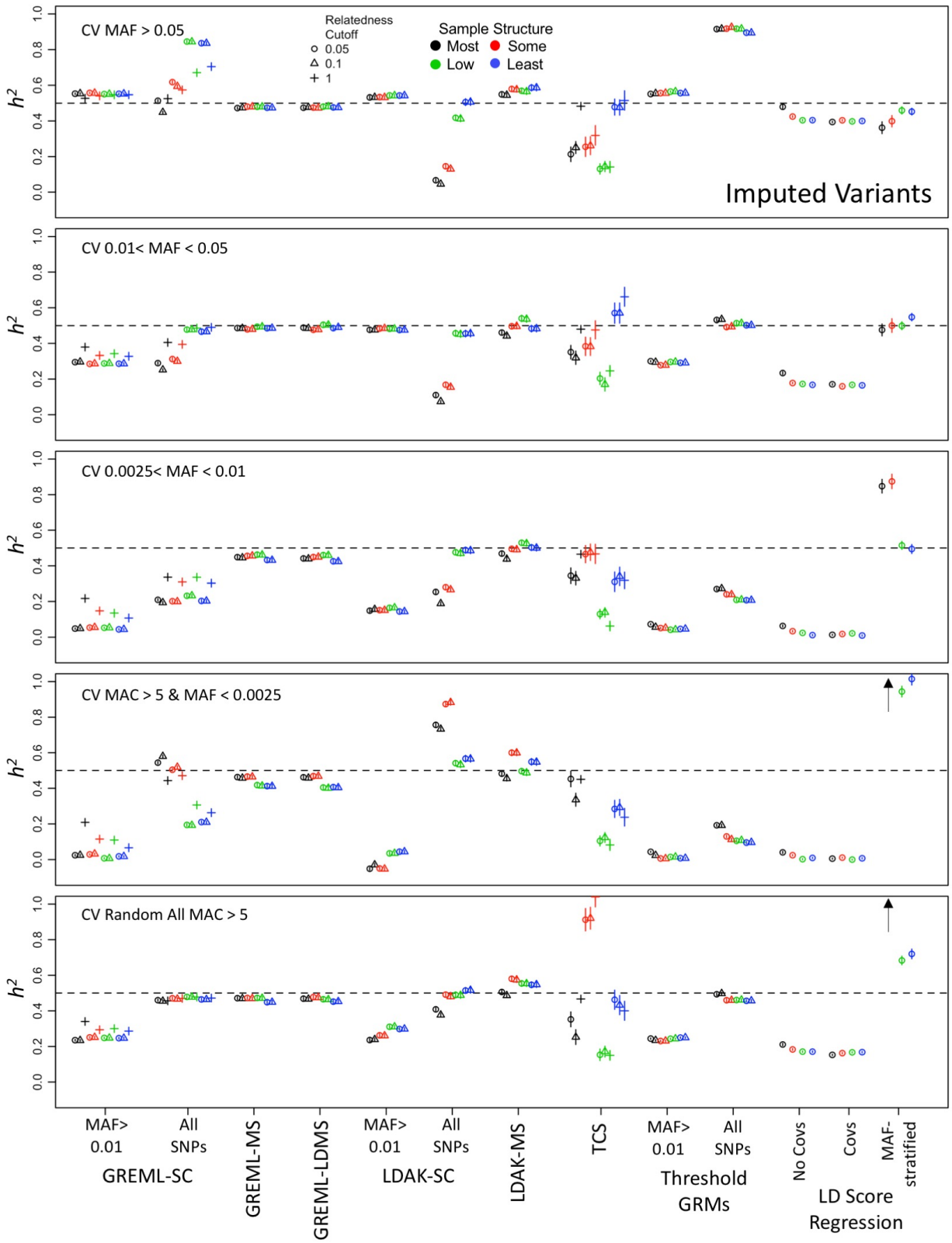


Figure S6. Narrow-sense heritability ($h^2$) estimates using imputed variants. Each horizontal panel indicates the minor allele frequency (MAF) range of the 1,000 randomly chosen causal variants (CV), with the range specified in the inset. Methods are listed on the X-axis as follows: Single component GREML (GREML-SC), MAF-stratified GREML (GREML-MS), LD- & MAF-stratified GREML (GREML-LDMS), Single-component Linkage Disequilibrium-Adjusted Kinships (LDAK-SC), MAF-stratified LDAK (LDAK-MS), Treelet Covariance Smoothing (TCS), Extended Genealogy with Thresholded GRMs, and LD Score Regression using no PCs as covariates in GWAS or using PCs as covariates. Symbols represent different relatedness cutoffs (or threshold, *t*, using the Threshold GRMs method). Dotted line is the simulated (true) $h^2$ = 0.5. Mean (±SEM) of 100 replicates shown. Colors represent the 4 subsamples varying in genetic structure. Estimates >1 are indicated by arrow.

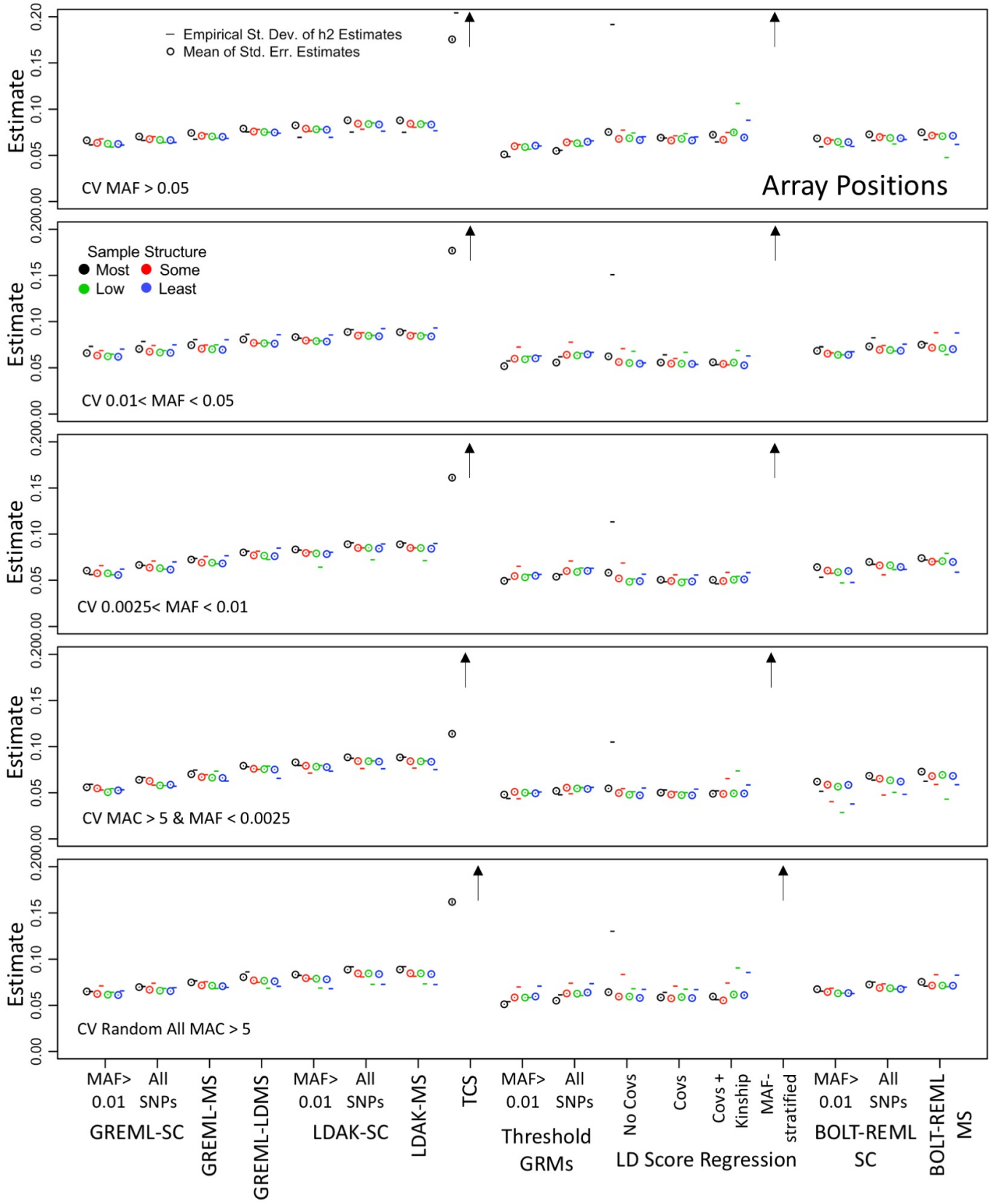


Figure S7. Using Axiom array positions, the estimates of the empirical standard deviation of the h2 estimates (-) from 100 replicates and the mean of the estimated standard error from the individual replicates (o). Shown are results using individuals with a relatedness cutoff of <0.05; results for relatedness <0.1 nearly identical and not shown. Most TCS and MAF-partitioned LD score regression estimates >0.2. Estimates >0.2 are indicated by arrow.

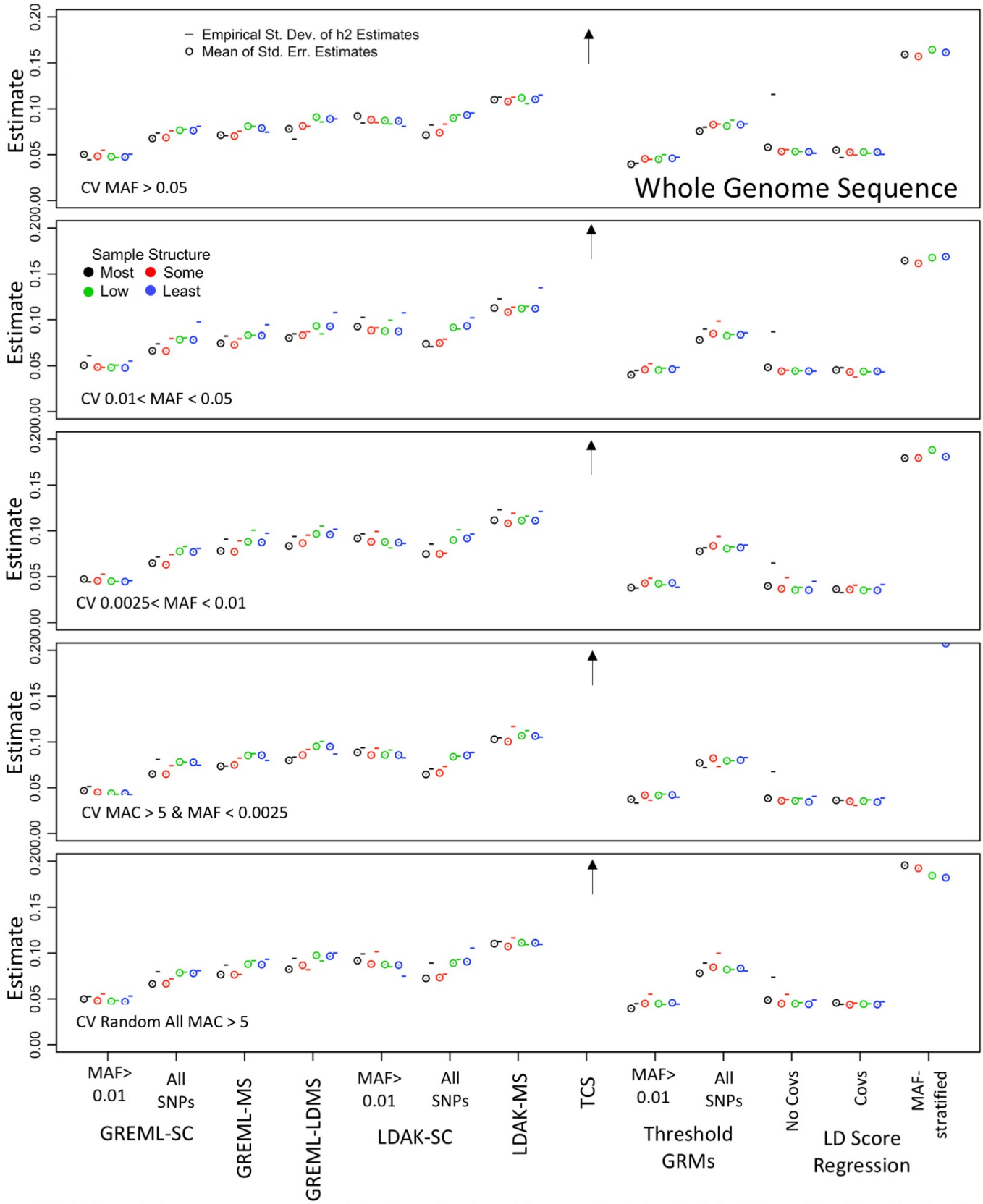


Figure S8. Using whole genome sequence data, the estimates of the empirical standard deviation of the h2 estimates (-) from 100 replicates and the mean of the estimated standard error from the individual replicates (o). Shown are results using individuals with a relatedness cutoff of <0.05; results for relatedness <0.1 nearly identical and not shown. Most TCS and MAF-partitioned LD score regression estimates >0.2. Estimates >0.2 are indicated by arrow.

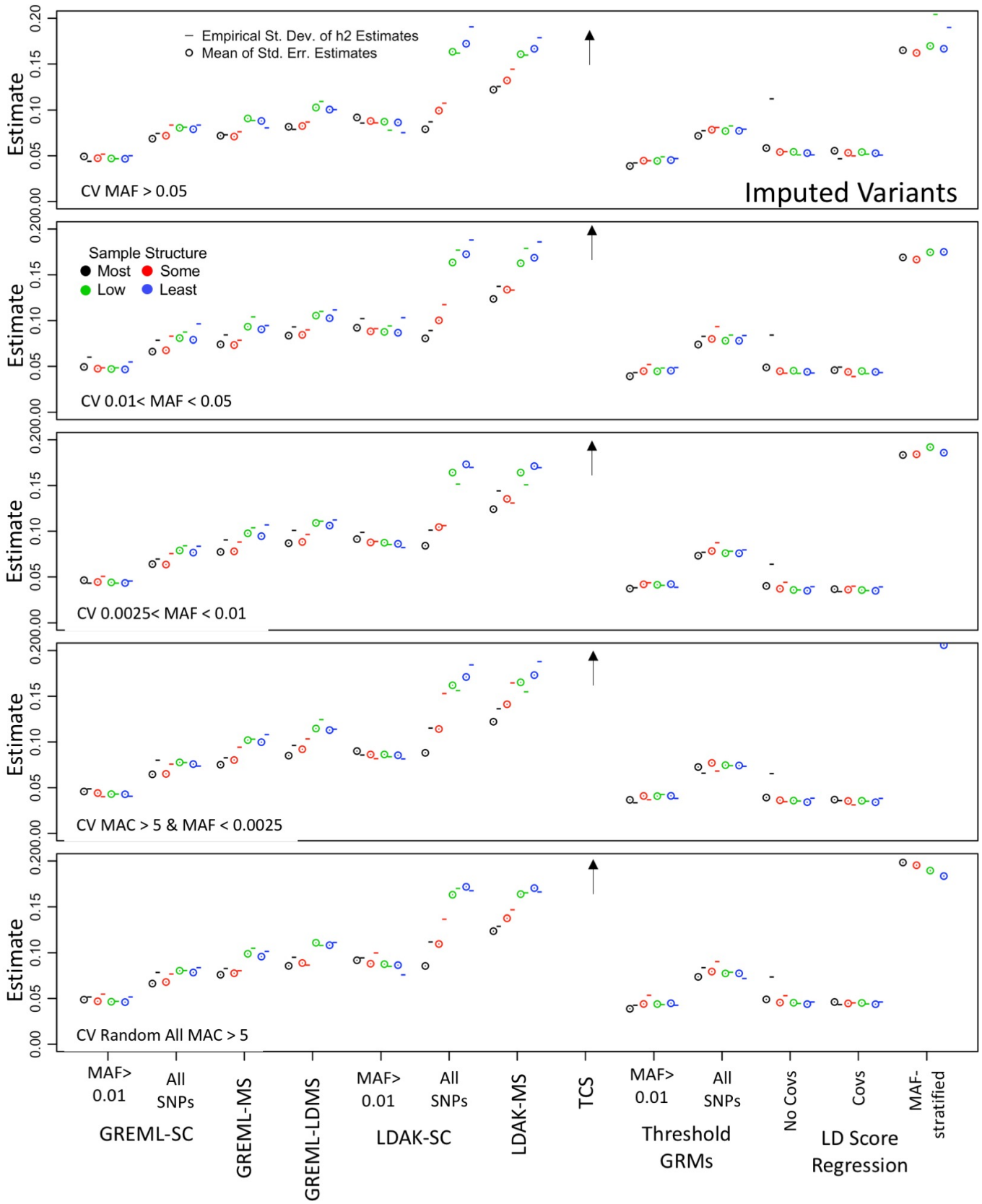


Figure S9. Using imputed variants, the estimates of the empirical standard deviation of the h2 estimates (-) from 100 replicates and the mean of the estimated standard error from the individual replicates (o). Shown are results using individuals with a relatedness cutoff of <0.05; results for relatedness <0.1 nearly identical and not shown. Most TCS and MAF-partitioned LD score regression estimates >0.2. Estimates >0.2 are indicated by arrow.

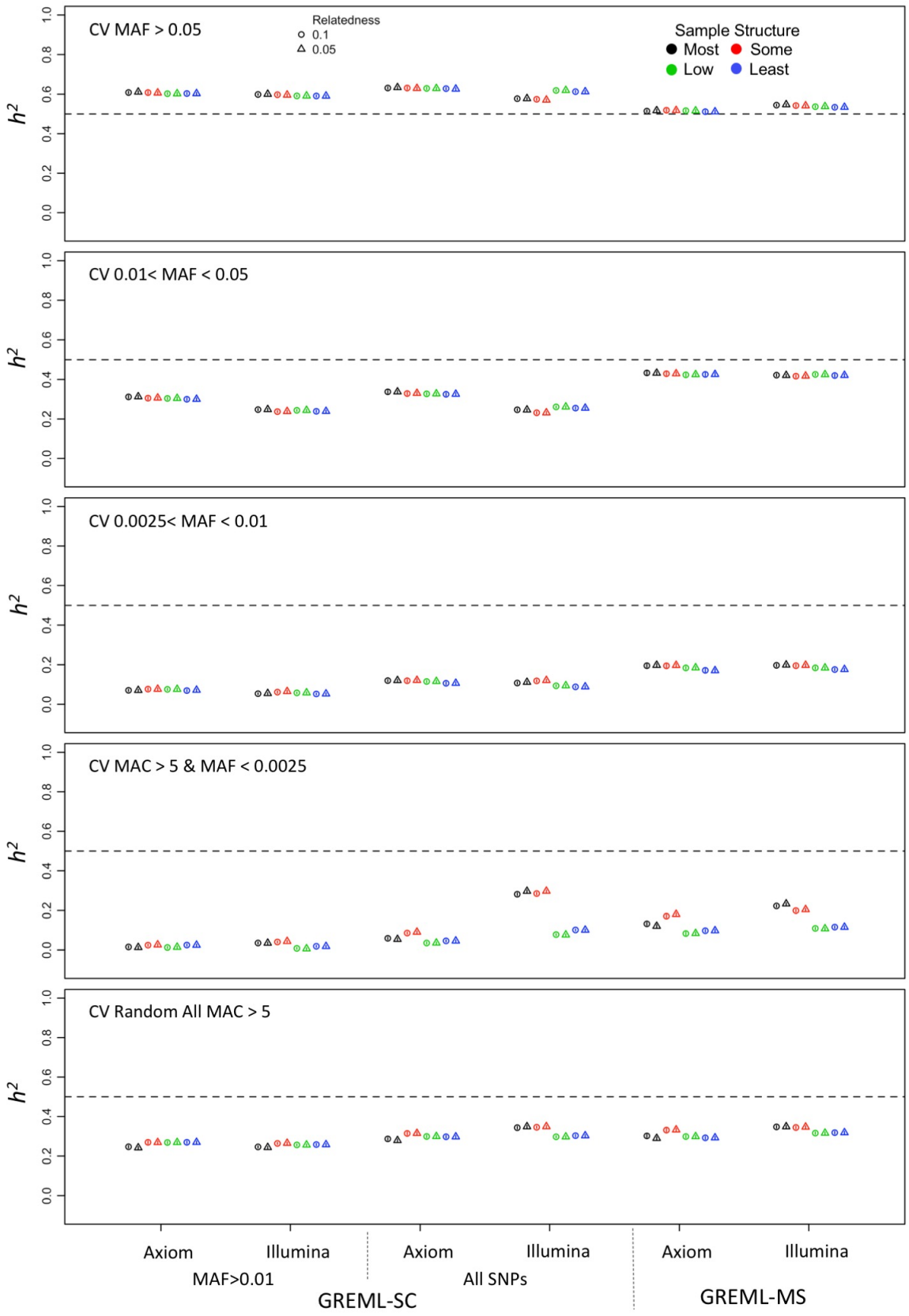


Figure S10. Narrow-sense heritability ($h^2_{SNP}$) estimates using commercial array positions from either the Affymetrix Axiom or the Illumina Omni2.5. Each horizontal panel indicates the minor allele frequency (MAF) range of the 1,000 randomly chosen causal variants (CV), with the range specified in the inset. Methods are listed on the X-axis as follows: Single component GREML (GREML-SC) with either only common SNPs (MAF>0.01) or all used to estimate the GRM, MAF-stratified GREML (GREML-MS). Symbols represent different relatedness cutoffs (or threshold, *t*, using the Threshold GRMs method). Dotted line is the simulated (true) $h^2$ = 0.5. Mean (±SEM) of 100 replicates shown. Colors represent the 4 subsamples varying in genetic structure.

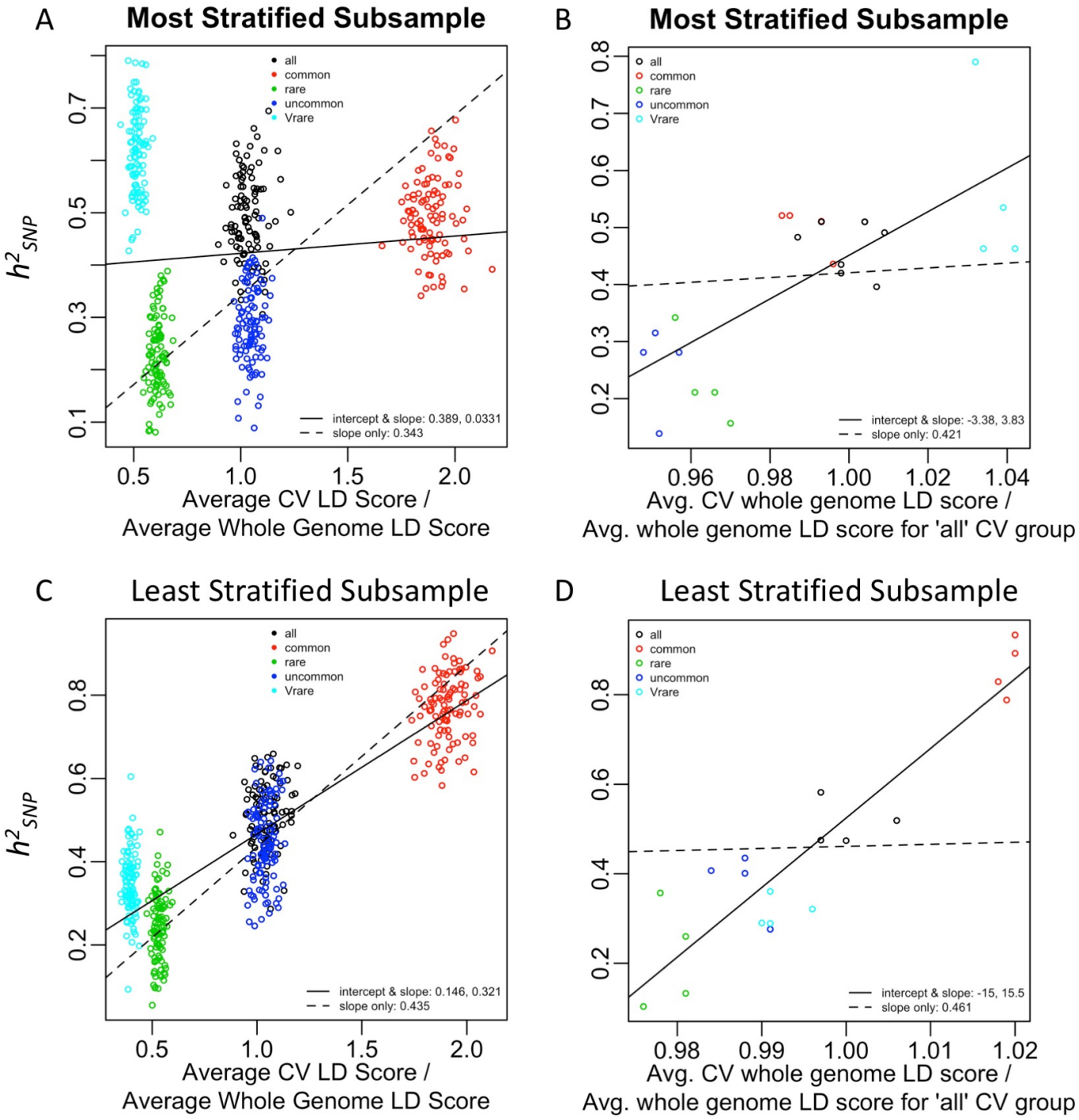


Figure S11. Using GREML-SC with GRMs developed from whole genome sequence data, $h^2_{SNP}$ is related to the LD between CVs and markers and the LD among all markers. In (A) and (C), $h^2_{SNP}$ is plotted against the average LD scores for CVs divided by the average LD scores for all whole genome sequence variants, using LD scores calculated in GCTA with window sizes of 100Kb for each of the 100 replicates for each CV MAF range, indicated by different colors. In unstratified samples, the relationship is close to the theoretical expectation (Yang et al. 2015). It fails in the most stratified subsample, presumably because of long-range LD for very rare markers. In (B) and (D), for 4 replicates of each MAF range, we calculated all pairwise $r^2$ estimates between the CVs and the rest of the genome (>16M per CV). Because we could not estimate all pairwise $r^2$ values for all whole genome sequence variants (>270 trillion estimates) for the denominator, we used the average from the 'all' CV group, which were 1,000 markers randomly chosen from all whole genome sequence variants. While the slope is not as expected (0.5), the relationship with LD is clear in both stratification subsamples. In all plots, the slope and coefficients are shown from linear regression, including when the intercept was fixed to 0.

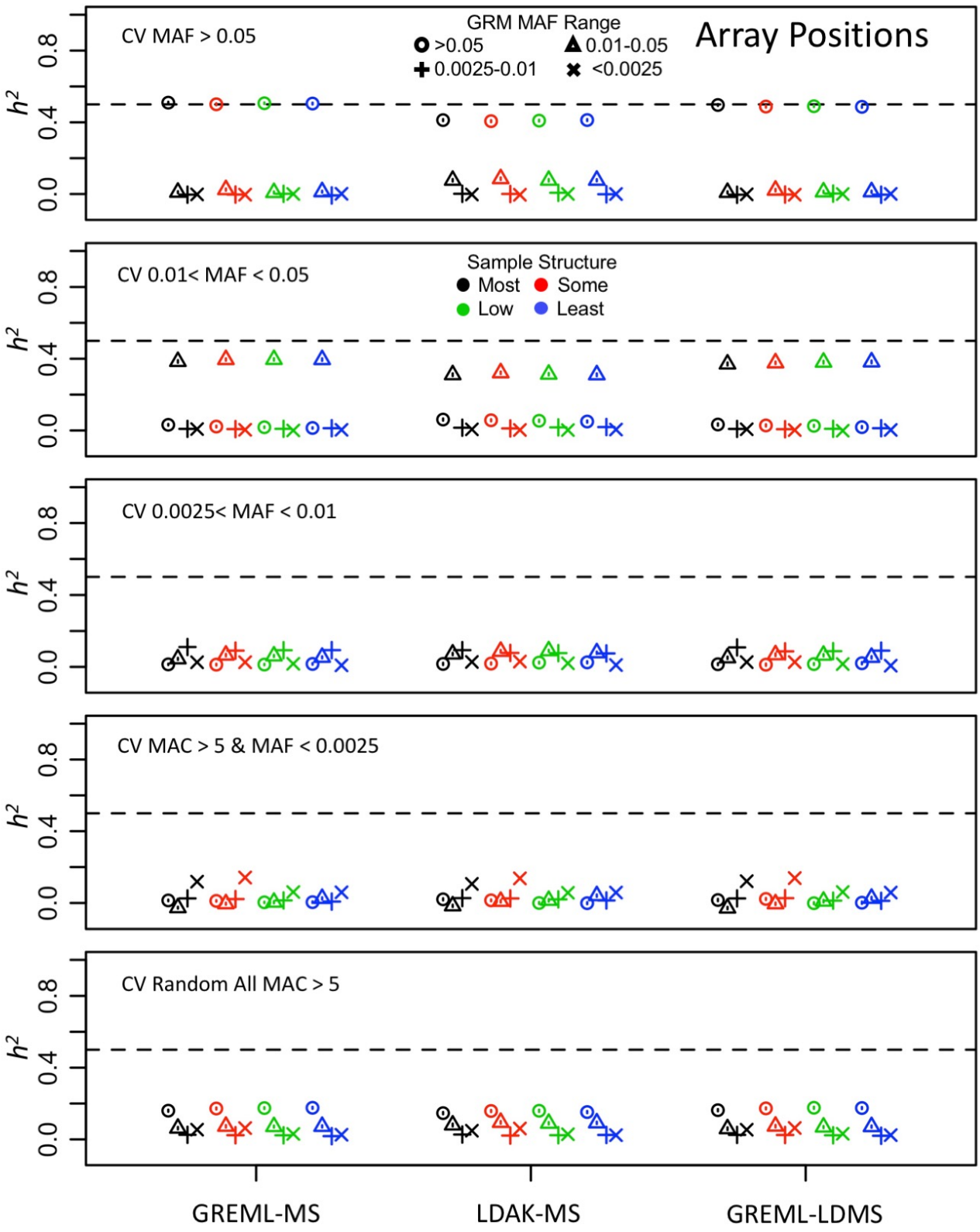


Figure S12. Methods to partition variance using array position SNPs. Shown are mean ± 1SEM from 100 repetitions. Each horizontal panel indicates the minor allele frequency (MAF) range of the 1,000 randomly chosen causal variants (CV), with the range specified in the inset. Symbols represent the MAF range of each GRM in the model, while colors represent the four population structure subsamples. Shown are results using individuals with a relatedness cutoff of <0.05; results for relatedness <0.1 nearly identical and not shown.

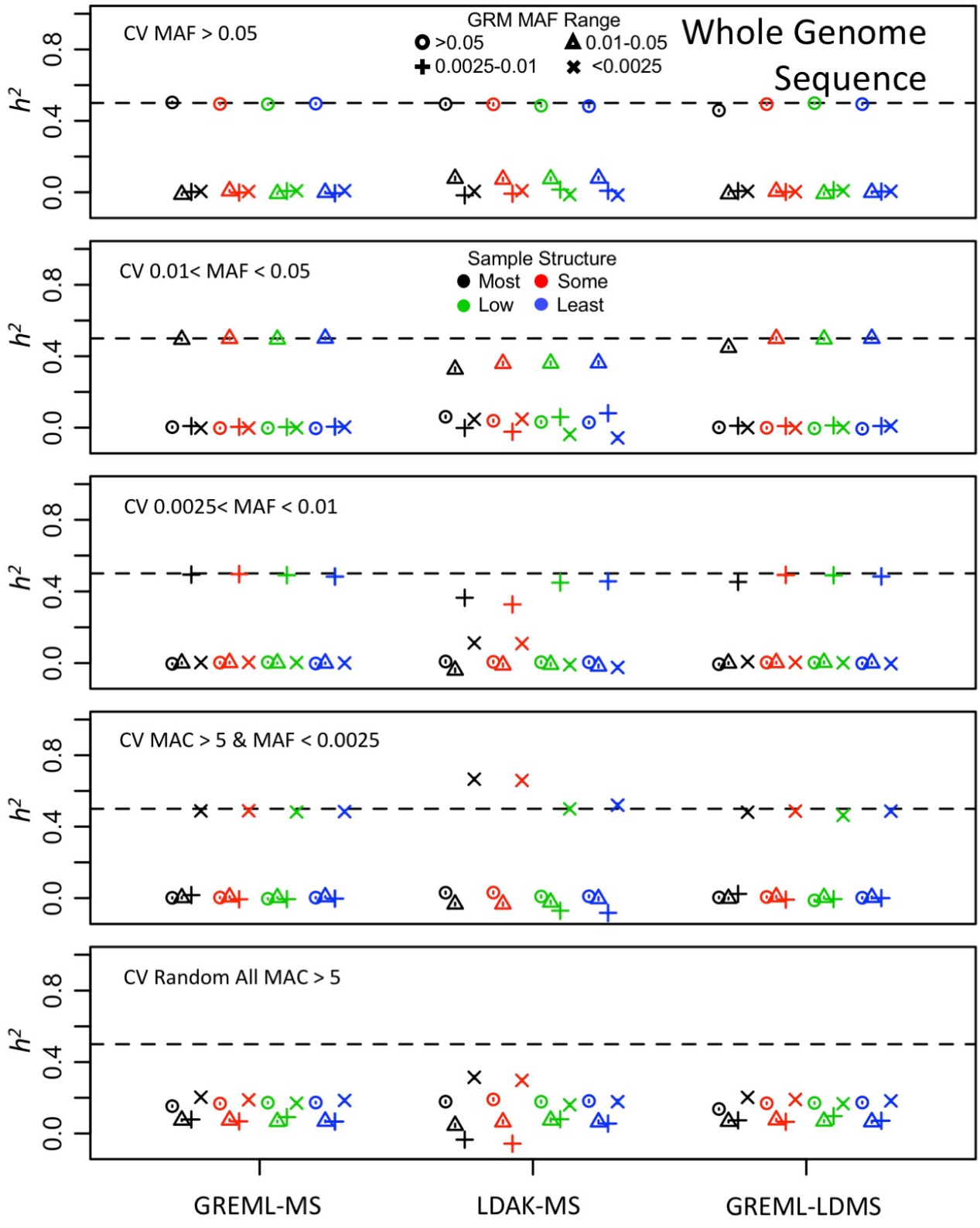


Figure S13. Methods to partition variance using whole genome sequence data. Shown are mean ± 1SEM from 100 repetitions. Each panel indicates the minor allele frequency (MAF) range of the 1,000 randomly chosen causal variants (CV). Symbols represent the MAF range of each GRM in the model, while colors represent the four population structure subsamples. Shown are results using individuals with a relatedness cutoff of <0.05; results for relatedness <0.1 nearly identical and not shown.

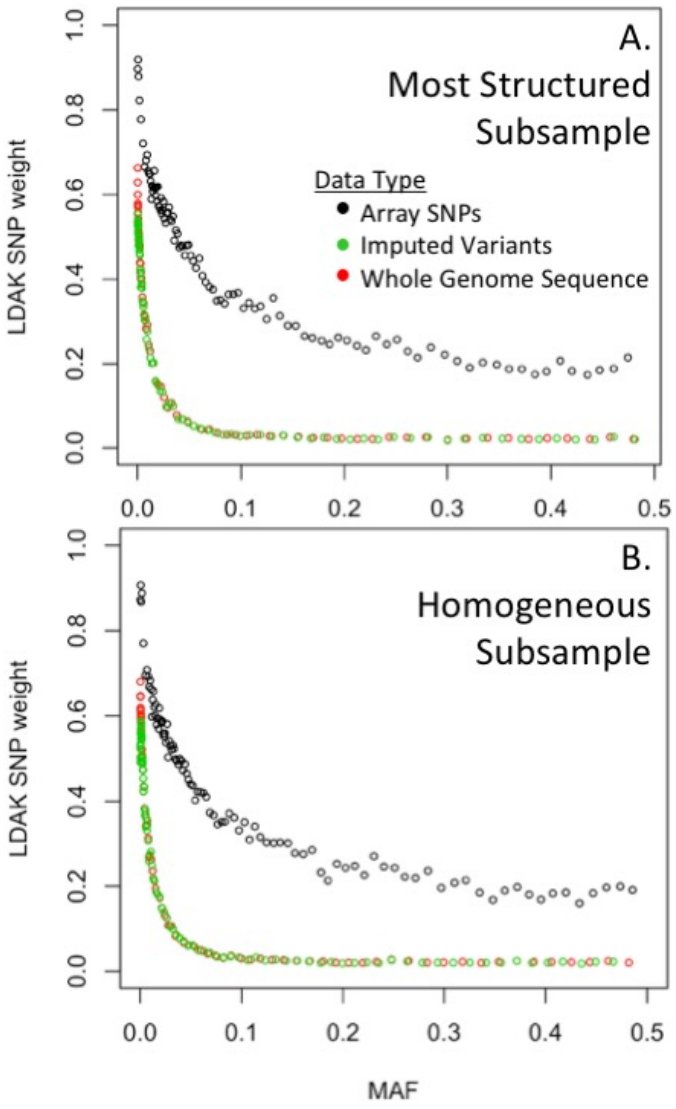


Figure S14. The relationship between the proportion of variants for each of 100 MAF bins, and the average LDAK SNP weights for each of 100 MAF bins (insets) for the most structured subsample (A) and the most homogeneous subsample (B). Only chromosome 22 variants shown.

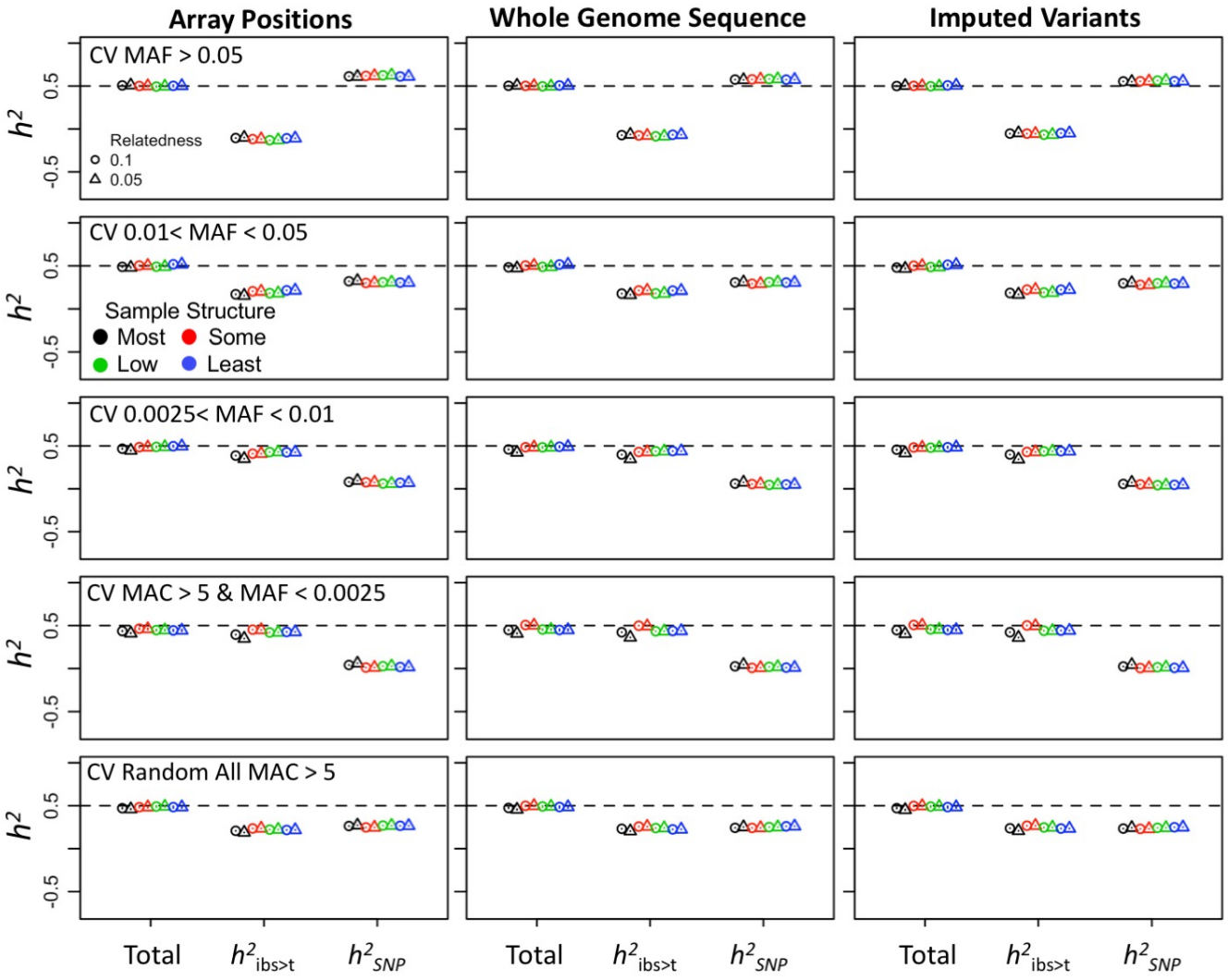


Figure S15. Total and partitioned variance estimates from the extended genealogy thredsholded GRMs, using variants with minor allele frequency > 0.01 with array position SNPs, whole genome sequence variants, or imputed genome-wide variants as indicated above each column of panels. On the x axis, Total indicates the sum of both variance component estimates and is the total $h^2$ estimate, $h^2_{ibs>t}$ is the variance attributed to the thresholded GRM, and $h^2_{SNP}$ is the variance attributed to the full, unthresholded GRM. Shown are mean ± 1SEM from 100 repetitions. Each horizontal panel indicates the minor allele frequency (MAF) range of the 1,000 randomly chosen causal variants (CV), with the range specified in the inset. Symbols represent the relatedness value threshold below which the GRM was set to 0, while colors represent the four population structure subsamples.

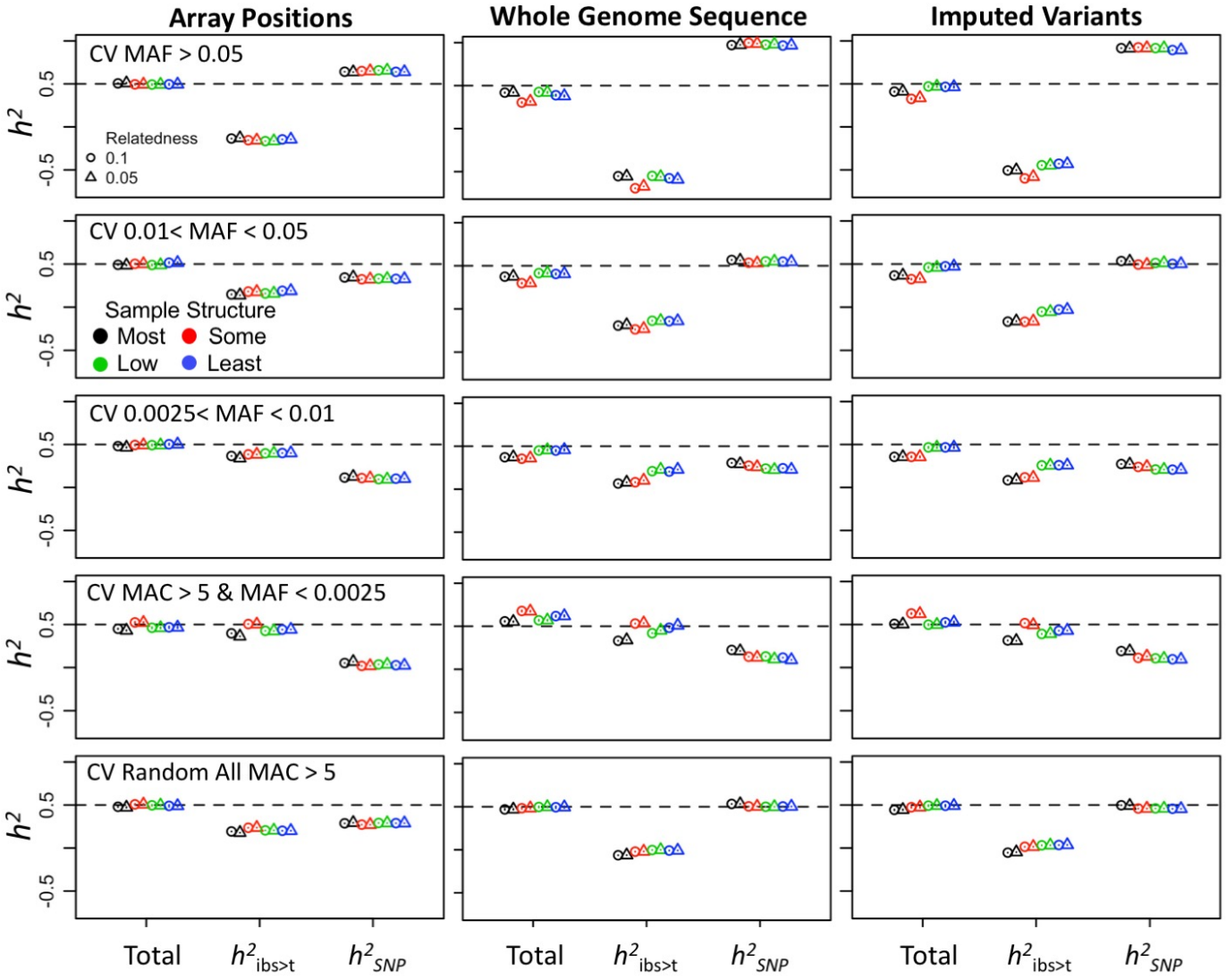


Figure S16. Total and partitioned variance estimates from the extended genealogy thredsholded GRMs, using all variants with array position SNPs, whole genome sequence variants, or imputed genome-wide variants as indicated above each column of panels. On the x axis, Total indicates the sum of both variance component estimates and is the total $h^2$ estimate, $h^2_{ibs>t}$ is the variance attributed to the thresholded GRM, and $h^2_{SNP}$ is the variance attributed to the full, unthresholded GRM. Shown are mean ± 1SEM from 100 repetitions. Each horizontal panel indicates the minor allele frequency (MAF) range of the 1,000 randomly chosen causal variants (CV), with the range specified in the inset. Symbols represent the relatedness value threshold below which the GRM was set to 0, while colors represent the four population structure subsamples.

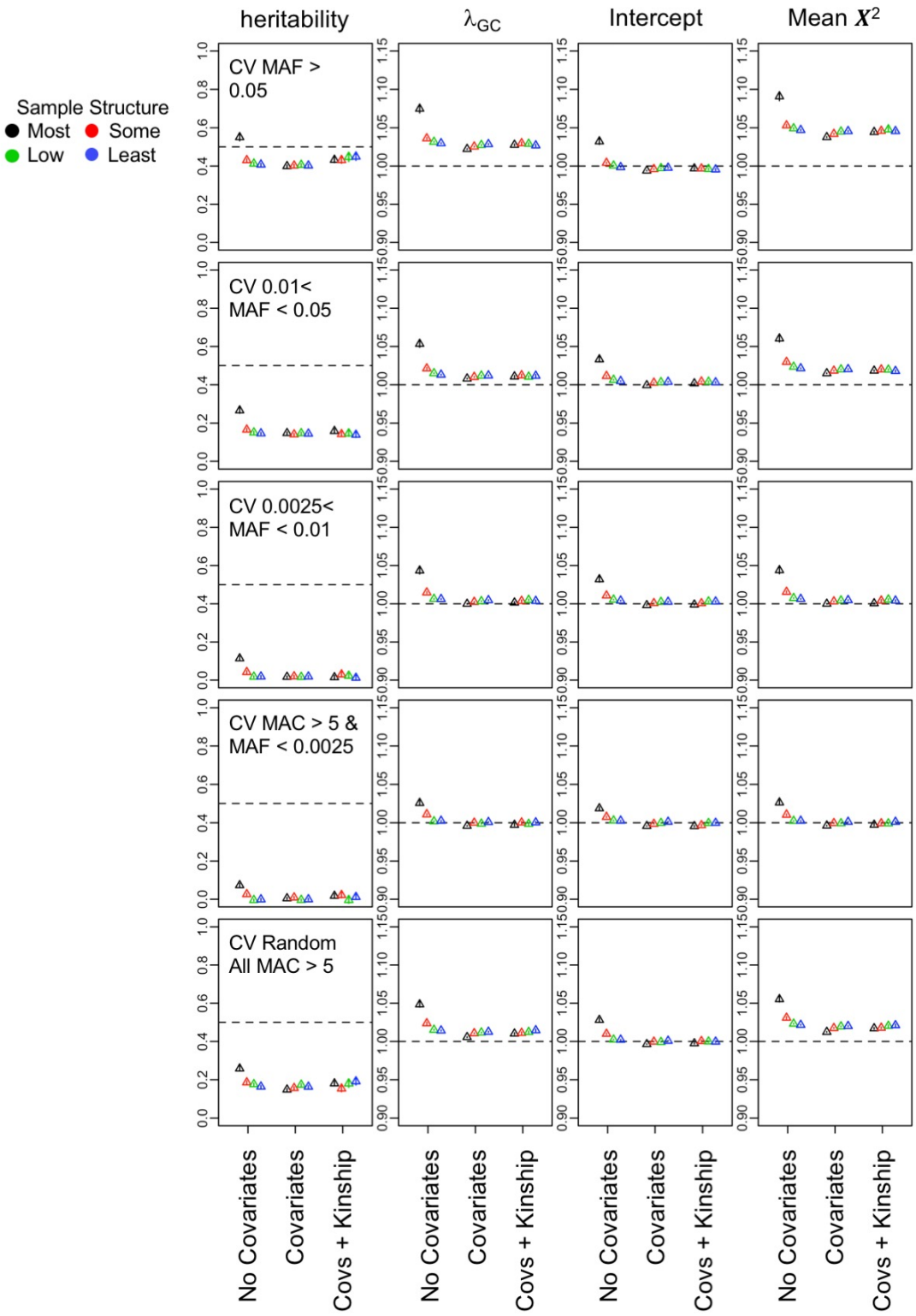


Figure S17. Using array position common SNPs, LD score regression estimates of heritability, genomic control inflation factor ($\lambda_{GC}$), regression intercept, and mean $X^2$ value as indicated above each vertical column of panels. Y-axis depends on the metric, as indicated by the column heading. On the x axis, the different approaches to handling confounding, with either no covariates, PC and sequencing cohort covariates included, or both covariates and a kinship matrix using the GCTA-LOCO approach. Shown are mean ± 1SEM from 100 repetitions. Each horizontal panel indicates the minor allele frequency (MAF) range of the 1,000 randomly chosen causal variants (CV), with the range specified in the inset. Colors represent the four population structure subsamples.

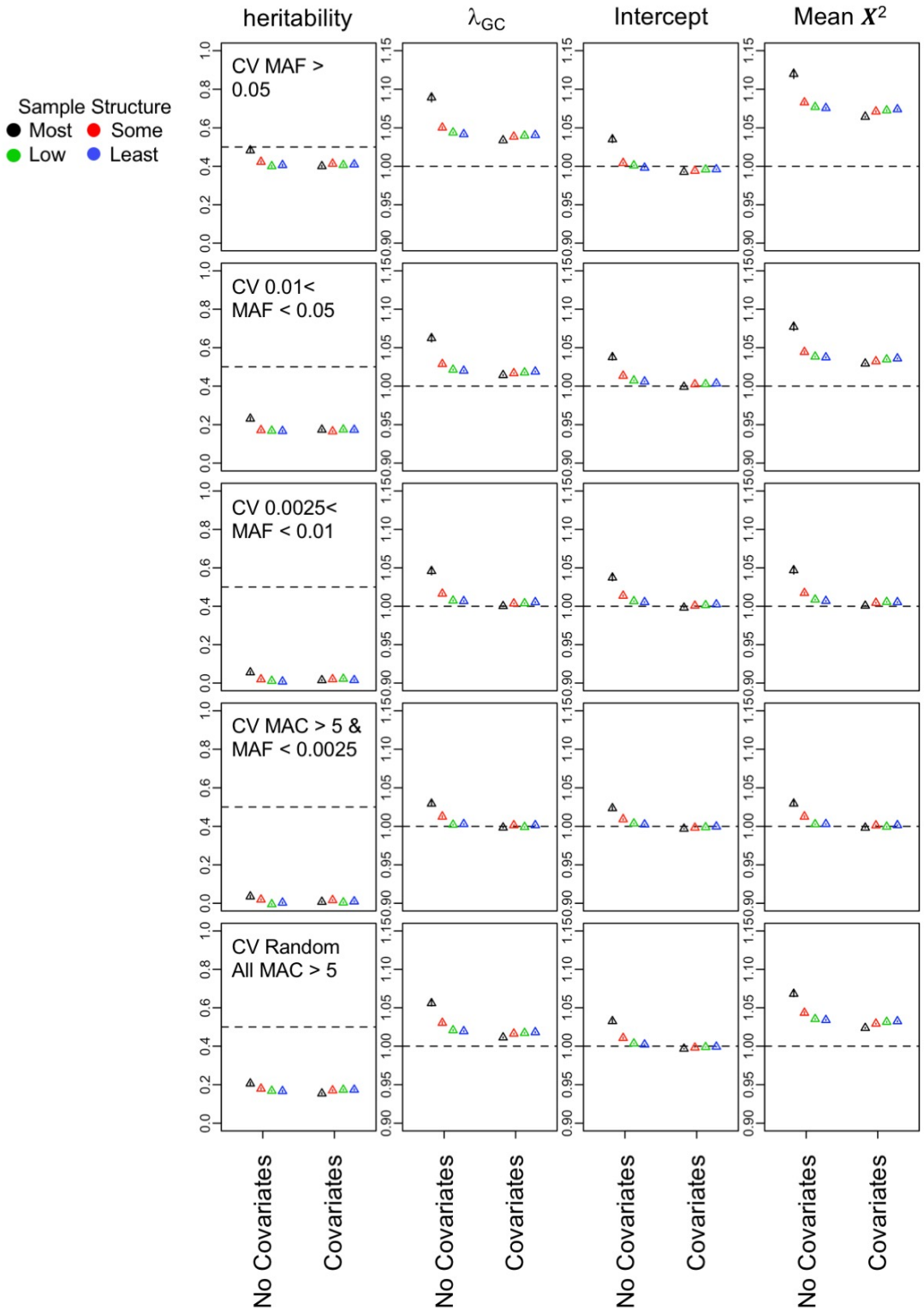


Figure S18. Using whole genome sequence common variants, LD score regression estimates of heritability, genomic control inflation factor ($\lambda_{GC}$), regression intercept, and mean $\boldsymbol{X}^2$ value as indicated above each vertical column of panels. Y-axis depends on the metric, as indicated by the column heading. On the x axis, the different approaches to handling confounding, with either no covariates or PCs and sequencing cohort covariates included. Shown are mean ± 1SEM from 100 repetitions. Each horizontal panel indicates the minor allele frequency (MAF) range of the 1,000 randomly chosen causal variants (CV), with the range specified in the inset. Colors represent the four population structure subsamples.

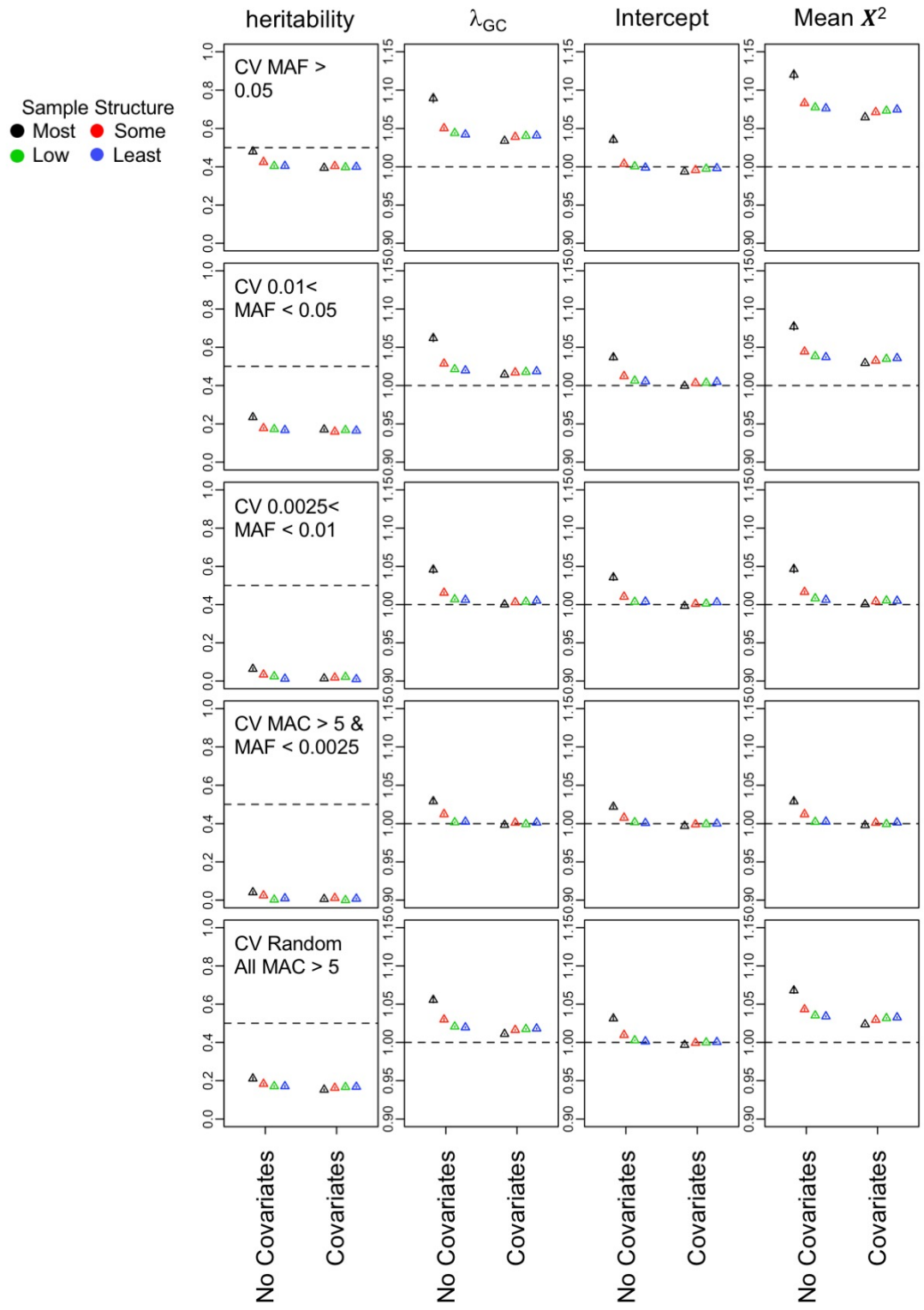


Figure S19. Using imputed genome-wide common variants, LD score regression estimates of heritability, genomic control inflation factor ($\lambda_{GC}$), regression intercept, and mean $\boldsymbol{X}^2$ value as indicated above each vertical column of panels. Y-axis depends on the metric, as indicated by the column heading. On the x axis, the different approaches to handling confounding, with either no covariates or PCs and sequencing cohort covariates included. Shown are mean ± 1SEM from 100 repetitions. Each horizontal panel indicates the minor allele frequency (MAF) range of the 1,000 randomly chosen causal variants (CV), with the range specified in the inset. Colors represent the four population structure subsamples.

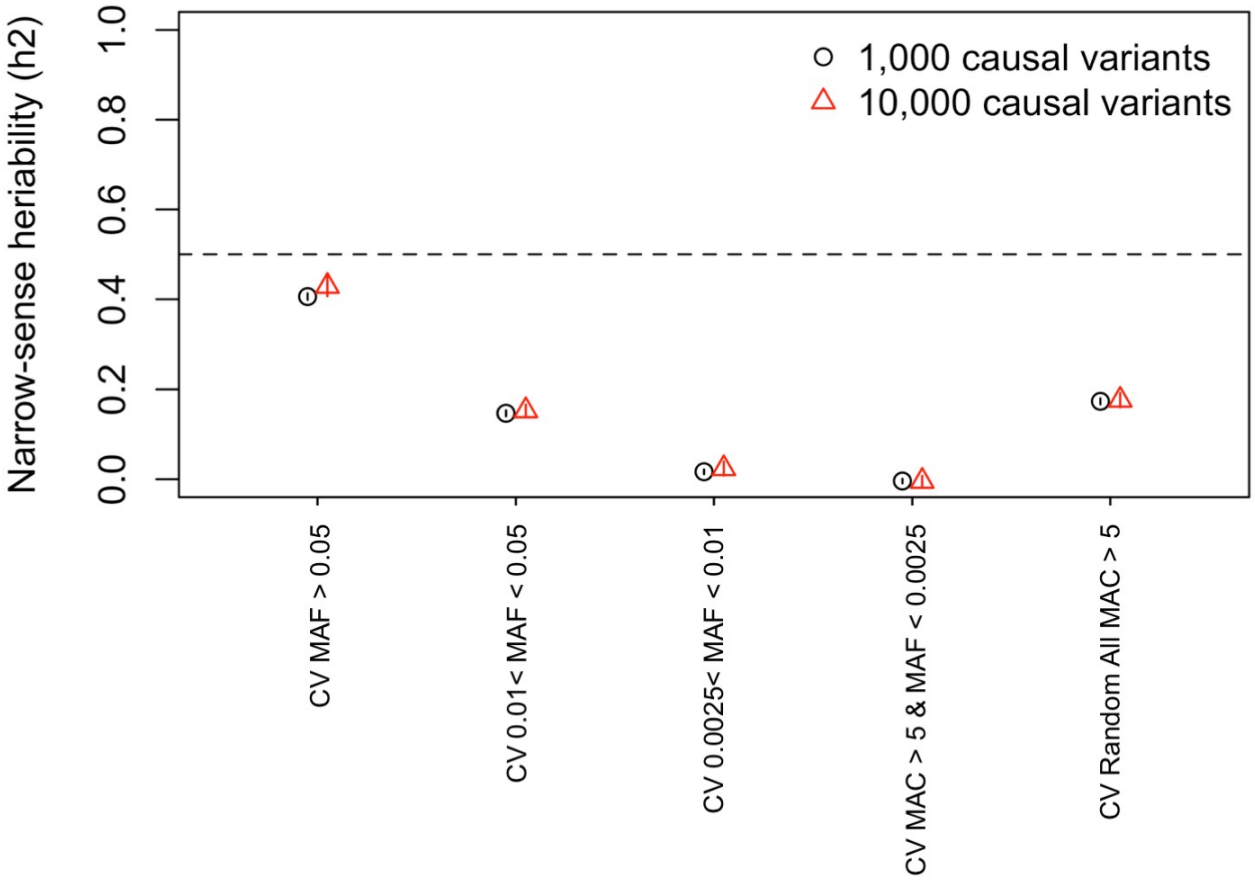


Figure S20. Using array position common SNPs, LD score regression estimates of heritability for traits simulated from either 1,000 causal variants (CVs) or 10,000 CVs (symbols/colors) within the low structure population subsample only. Shown are mean ± 1SEM from 20 repetitions. X-axis indicates the minor allele frequency (MAF) range of the randomly chosen causal variants (CV). In these simulations, PC scores and sequencing cohort were used as covariates in the GWAS.

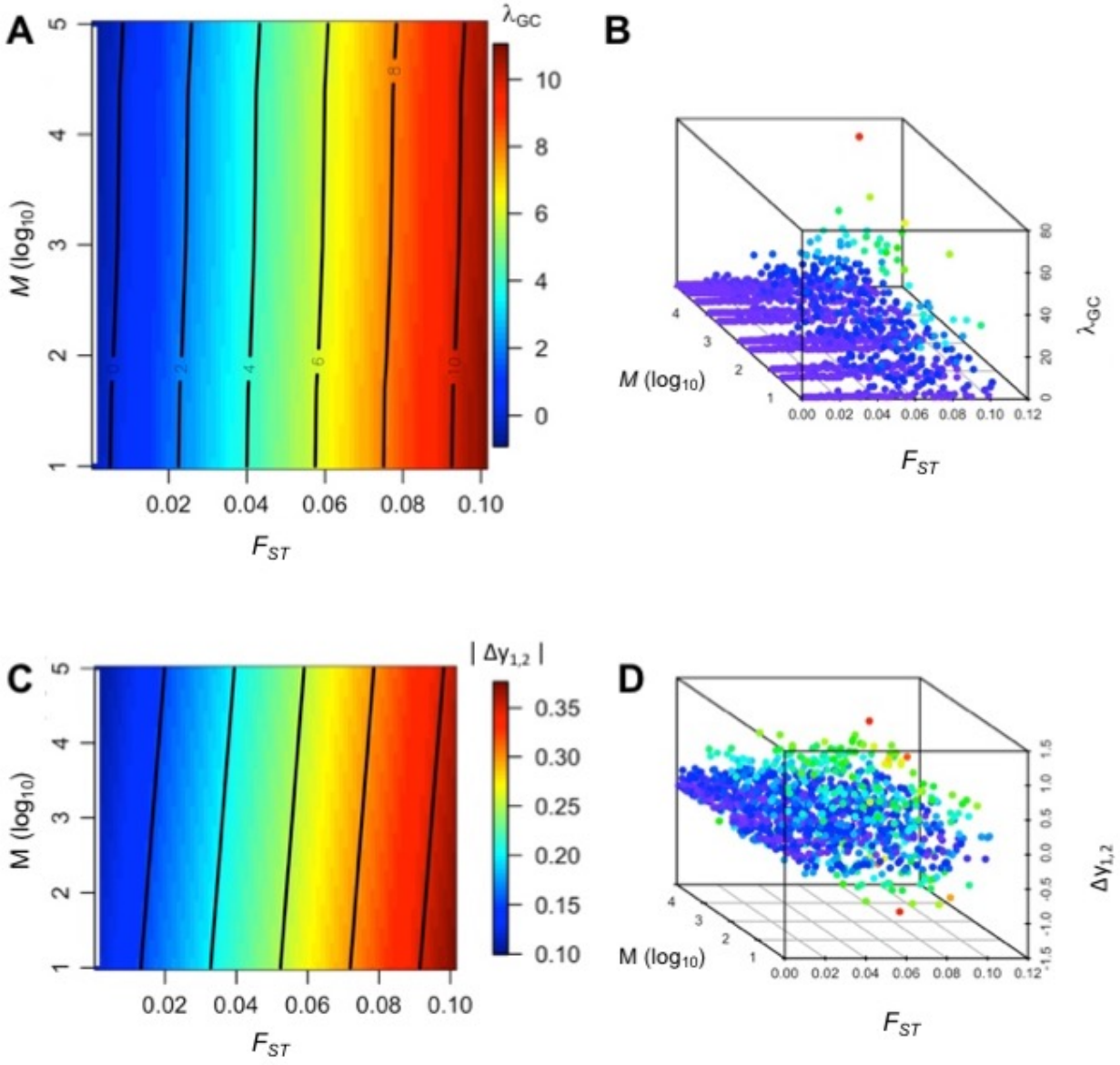


Figure S21. Genomic control inflation factor, $\lambda_{GC}$ as a function of $F_{ST}$ and the number of causal variants $M$ (A, B), and the mean difference in liability between two populations ($\Delta y_{1,2}$) (C, D). To confirm that the inflation of $\lambda_{GC}$ was due to structure rather than spurious results, we simulated a simple case/control GWAS dataset, testing common simulated SNPs from two populations with varying degrees of structure ($F_{ST}$) and polygenicity. We simulated genotypes as in Zaitlen et al. (2014) from two populations (N=2,000 individuals in each) using $h^2$ = 0.5. We created phenotypes for $M$ = 10, 50,100, 500, 1000, 5000, 10000, 25000, 50000, 75000, and 100000 causal variants. We repeated this process for $F_{ST}$ between 0.001 and 0.101, in increments of 0.001. We created independent sets of 10,000 unassociated markers for each of the phenotypic datasets created under different levels of polygenicity and differentiation ($F_{ST}$), creating null sets of markers to determine if $\lambda_{GC}$ was inflated under the true null hypothesis of no association. We tested each of the 10,000 unassociated markers for association using an Armitage Trend test. The figure demonstrates that when there is no true association, increasing levels of $F_{ST}$ lead to inflation of $\lambda_{GC}$ (A, B). This is due to the larger variability in the mean difference in liability between the populations (C, D). It should be noted that the expected mean liability difference between populations is still zero, and that is the observed mean across the range of values we simulated. However, the variance increases with larger $F_{ST}$, leading to chance, stronger associations when the allele frequencies of unassociated test markers differ between the two populations. Increasing polygenicity mitigates this effect to some extent, particularly at $F_{ST}$ levels observed commonly within GWAS datasets. However, the impact of higher $F_{ST}$ appears to outweigh the impact of more causal markers. Inflation of $\lambda_{GC}$ is eliminated when the phenotypes are drawn from distributions with the same mean (e.g., normally-distributed liability scores with mean 0, unit variance, or an equal number of cases/controls in each population). Thus, when no chance phenotypic difference exists between population means, the inflation vanishes. Importantly, environmental factors that vary among populations will also lead to spurious associations, a point well established that we did not simulate here. Thus, confounding effects of population stratification require careful control when estimating $h^2$ from GWAS statistics, or evaluating the GWAS statistics themselves.

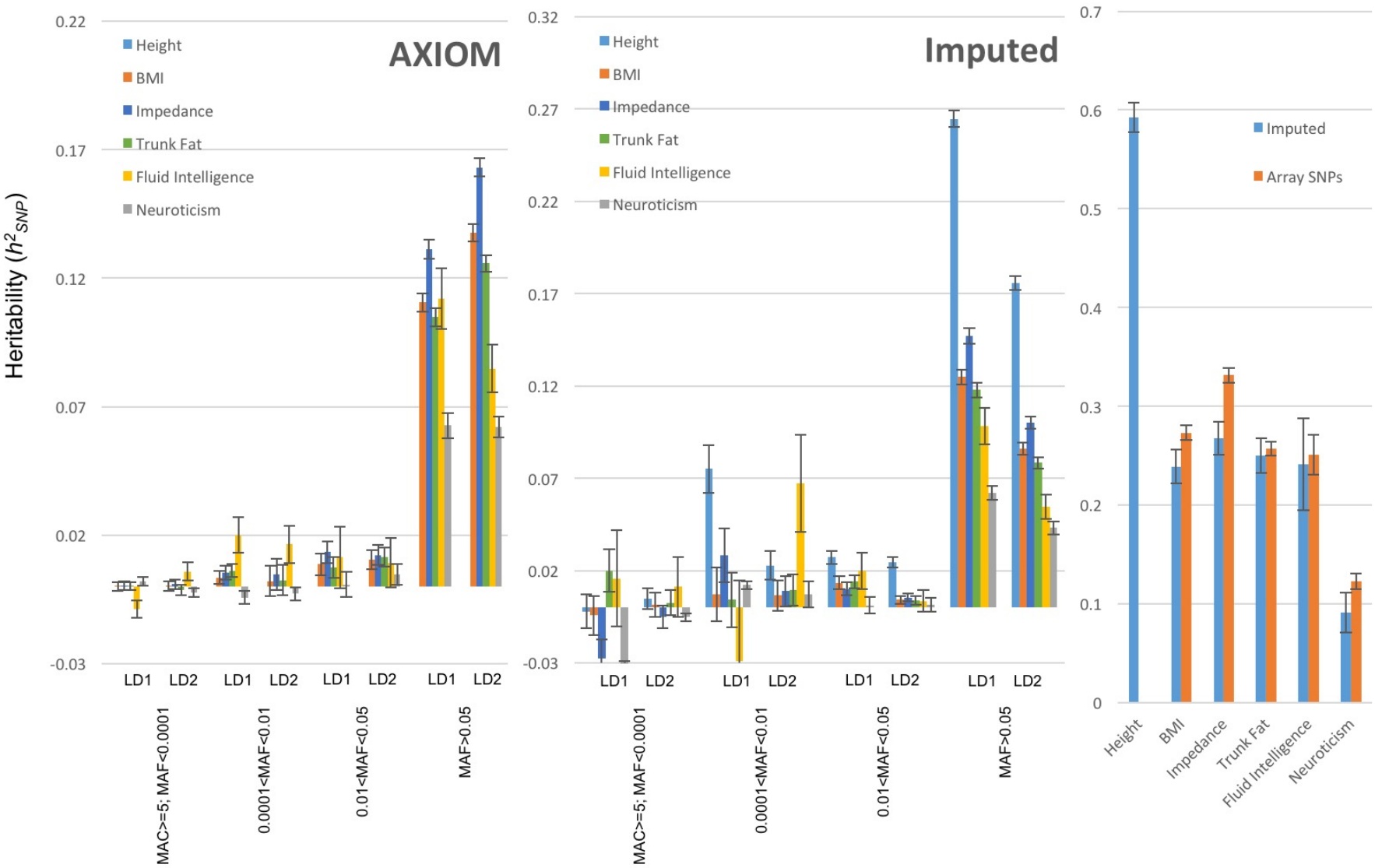


Figure S22. UK Biobank heritability estimates for six complex traits. $h^2_{SNP}$ using GREML-LDMS with Axiom array SNPs (left), or imputed genome-wide variants (center), showing estimates for each MAF range. Total $h^2_{SNP}$ shown on right. In left and center panels, x-axis indicates the MAF range and LD score half of each of the 16 GRMs used in the GREML-LDMS model. The information matrix was not invertible for height using the Axiom positions; no estimates were produced.